International Journal of Solids and Structures 51 (2014) 402–415

Contents lists available at ScienceDirect

International Journal of Solids and Structures

journal homepage: www.elsevier.com/locate/ijsolstr

Effect of nonlinear strain paths on forming limits under isotropic and anisotropic hardening

Ji He [a,b], Danielle Zeng [c], Xinhai Zhu [d], Z. Cedric Xia [c,*], Shuhui Li [a,b]

[a] State Key Laboratory of Mechanical System and Vibration, Shanghai 200240, China
[b] Shanghai Key Laboratory of Digital Manufacture for Thin-walled Structures, Shanghai Jiao Tong University, Shanghai 200240, China
[c] Ford Motor Company, Dearborn, MI, USA
[d] Livermore Software Technology Corporation, Livermore, CA, USA

ARTICLE INFO

Article history:
Received 9 May 2013
Received in revised form 7 October 2013
Available online 18 October 2013

Keywords:
Constitutive behavior
Marciniak–Kuczynski analysis
Stability and bifurcation
Forming Limit Diagram

ABSTRACT

The path-dependence of the conventional Forming Limit Diagram (FLD) is an important issue for its applications in industry. Great efforts have been made to understand the nature of the path-dependence with both experimental and theoretical approaches, many of them attempting to find a path-independent way for the application of forming limits. In this paper, we focus on the nonlinear strain path effect on forming limit predictions using both isotropic and anisotropic hardening models. The Forming Limit Diagram (FLD), Forming Limit Stress Diagram (FLSD) and Forming Limit Effective Strain Diagram (epFLD) of sheet metals subject to linear and nonlinear strain paths are analyzed and compared using the Marciniak–Kuczynski approach. An anisotropic hardening model based on Yoshida and Uemori development is adopted in this study, and it is coupled with the traditional Hill'48 yield surface. This model is capable of describing the complex Bauschinger phenomenon after the material undergoes the reverse loading process such as the early re-yielding, work-hardening stagnation and permanent softening. Two different scenarios for the change of strain paths are also investigated. In the first scenario, the sheet material is initially loaded with a fixed strain increment ratio, unloaded to the free stress state, and then reloaded with a different strain increment ratio until the forming limit is reached. In the second scenario, the material does not undergo elastic unloading. Instead, the strain path is abruptly changed to a different strain increment ratio and the material undergoes continuous loading until the forming limit is reached. It is found that the work-hardening behavior after the pre-straining and the loading scenario plays an important role in the path dependent behavior of forming limits. Detailed analysis reveals that the M–K approach may have contributed to the significance of path-dependence observed in this study, especially at high pre-strain levels.

1. Introduction

The Forming Limit Diagram (FLD) is an essential tool to assess sheet metal formability in metal forming operations. The conventional strain based FLD pioneered by Keeler and Backhofen (1964) and Keeler (1965) has been widely used to access this onset of localized necking failure in sheet metal during material deformation, and normally determined by conducting Limiting Dome Height (LDH) tests such as Nakazima or Marciniak test where the strain path is largely linear. However, the material deformation in sheet metal forming processes is almost always nonlinear. In operations such as deep drawing under complex loading conditions, the loading paths can deviate significantly from linearity. Furthermore, in multi-stage forming processes, such as drawing followed by flanging, the loading direction will inevitably change. Numerous testing data (Laukonis and Ghosh, 1978; Lloyd and Sang, 1979; Friedman and Houston, 1999) showed that there is no single curve in strain space that can represent the forming limit under nonlinear loading conditions. Graf and Hosford (1993, 1994) also demonstrated experimentally the nature of path-dependence of FLD in strain space by measuring the limit strains of aluminum sheets under a two-step loading condition. Theoretically, Cao et al. (2000) and Yao and Cao (2002) used both isotropic and kinematic hardening models with a general anisotropic yield criterion to calculate the FLD under non-proportional strain paths. They compared their results with Graf and Hosford's experiments and found broadly good agreements.

Recently, stress-based forming limit diagram (SFLD) has received increasing attention as an alternative to the conventional strain-based FLD. It has the advantage of not depending on deformation paths, and can be conveniently converted from traditional strain-based FLDs. Stoughton (2000, 2001) calculated the limit stress state from the limit strain data under both proportional

* Corresponding author. Tel.: +1 313 845 2322; fax: +1 3133900514.
E-mail address: zxia@ford.com (Z. Cedric Xia).

0020-7683/$ - see front matter © 2013 Elsevier Ltd. All rights reserved.
http://dx.doi.org/10.1016/j.ijsolstr.2013.10.013

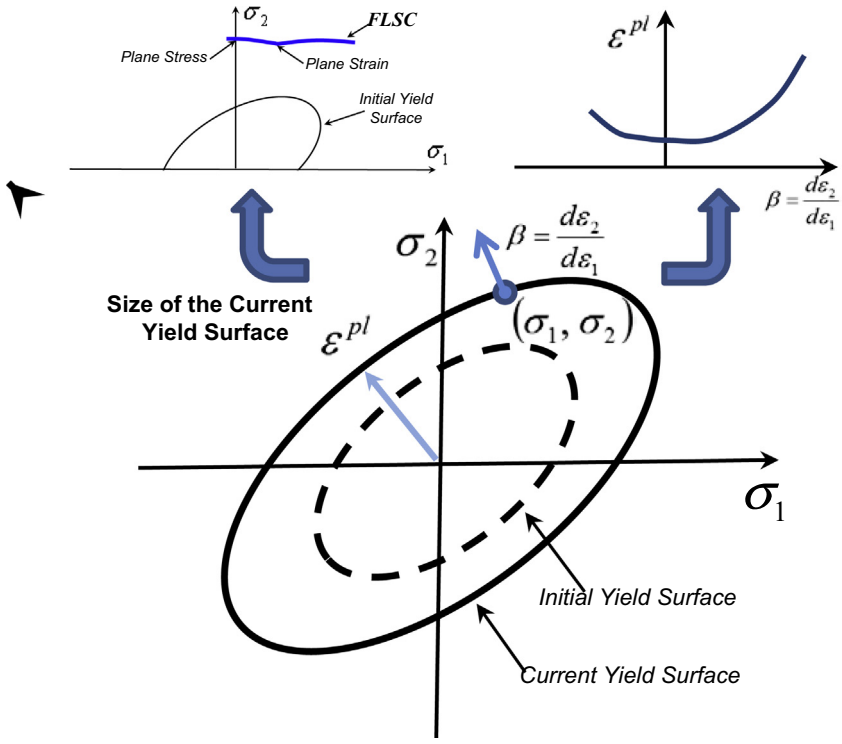

Fig. 1. Illustration of the path-independent forming limits under isotropic assumption.

and non-proportional loading conditions, and showed that the Forming Limit Stresses are largely insensitive to the strain path history. Stoughton and Zhu (2004) gave a review of theoretical models of the strain-based FLD and their relevance to stress-based FLD. They proposed several methods to translate the strain based FLD to stress spaces under the isotropic hardening assumption. Despite the attractiveness of the stress-based forming limit diagram, it has so far found limited applications in industrial practice. Several factors work against its wider acceptance. Firstly the classic forming limit diagram is deeply rooted in the practical world of circle grid analysis on the shop floor. Secondly, stresses are a more abstract concept and cannot be measured in any practical way when looking at a formed part. Thirdly, the accuracy in stress prediction is less reliable than for strain, even with the tremendous advances in numerical technology for sheet metal forming over the past decade.

Zeng et al. (2009) proposed a path-independent forming limit diagram based on effective strain and strain ratio (epFLD). In this approach, the stress states is described in terms of the size of current yield surface and current plastic flow direction. It is validated through both theoretical prediction with M–K analysis and available experimental data in literature (Friedman and Houston, 1999; Graf and Hosford, 1994). The epFLD is equivalent to stress-based forming limit diagram in all theoretical aspects as shown in Fig. 1, but differs in its presentation. It avoids issues with the reliability and oscillations of stress calculations associated with current software capabilities. It is relatively easy to implement into forming simulation software since it only requires strain results from the final two steps to calculate directions of strain increment. It should be noted that, in cases where a material point deforms beyond the necking criterion during a forming process but goes back under elastic deformation at the final stage of the deformation, both FLSD and epFLD will fail. But in epFLD, since only the plastic flow direction β is undetermined in this situation and the effective plastic strain is still available, it suggested to use a conservative estimate of assuming $\beta = 0$ for assessing the formability.

As we know, it is difficult to determine forming limits with changing strain path in the physical test. Furthermore, there are almost no direct measurement methods to determine the forming limits in stress space. Accordingly, few experimental tests have been conducted so far to validate path-independent Forming Limit Criteria. In recent years, Yoshida et al. (2005) measured the FLD and FLSD of aluminum AA5154-O through a servo-controlled testing machine under many linear and nonlinear stress paths. The path-independence of the FLSD was partially confirmed in their experimental results. Kuwabara et al. (2005) also measured the plastic deformation behavior of aluminum tubes. They found that the path-independent FLSD can be well predicted under the isotropic hardening assumption for nonlinear stress paths.

Some recent work showed that even the stress based FLD is path dependent under certain combined loading conditions. Yoshida et al. (2007) investigated the effect of changing strain paths on forming limit stresses using M–K model and a phenomenological plasticity model with non-normality under the isotropic hardening assumption. They discovered that with unloading between two loading steps, the forming limit stress is path independent. While without unloading, the limit stress clearly depends on the strain path history. Later, Yoshida and Kuwabara (2007) observed the forming limit strain and stress of steel tubes using a tension-internal pressure testing machine. They found out that whether the forming limit stress is path independent depends on the subsequent strain hardening behavior of the pre-strained material. The forming limit stress for combined stress path will coincide with FLSC under linear strain path with material following isotropic hardening rule, and it will lower when material exhibits a low strain hardening rate after strain path changes. Yoshida and Suzuki (2008) further studied the FLSD using M–K model with anisotropic hardening assumption. They concluded that stress based FLD is

path independent only for a material with a work hardening behavior that is not affected by strain path change.

Since the forming limit criterion is so critical in sheet metal formability assessment, it is thus very beneficial to have a path-independent criterion in order to assess the real formability of a formed part and not rely on the uncertain sense of security provided by a safety margin imposed on FLD in current industry practice to offset the path dependence. This paper aims to understand several basic questions: are FLSD and epFLD path-independent under isotropic and anisotropic hardening assumptions? If not, how significant is it and what are the implications in practice? Where does the differences come from, is it intrinsic or merely a result of M–K analysis?

Intensive studies have been conducted to model the cyclic behavior of sheet metals over the past decade. One of the notable work and widely adopted later by other researchers is carried out by Yoshida and Uemori (2002). In their paper, complex Bauschinger effect such as the early re-yielding, work-hardening stagnation and permanent softening are considered through a two-surface kinematic hardening constitutive model. This model is later modified by Shi et al. (2008) to avoid unrealistic work-hardening stagnation in scenario of steels, and is implemented in commercial software LS-DYNA. This modified Yoshida–Uemori model is adopted in this paper to investigate the effect of nonlinear strain paths on forming limits under isotropic and anisotropic hardening loading conditions. Two different loading procedures are considered. In the first scenario, the material is initially loaded with a fixed strain increment ratio, unloaded to free stress state, and then reloaded with a different strain increment ratio until the Forming Limit is reached; In the second scenario, the material does not undergo elastic unloading. Instead, the strain path is abruptly changed to a different strain increment ratio until the Forming Limit is reached. The Marciniak–Kuczynski (M–K) analysis is used as the framework to predict the forming limits. Hill'48 yield surface and flow theory are adopted for the purpose of understanding the nature of path-dependence of forming limits under isotropic and kinematic hardening, where in-plane transverse isotropy is used for simplicity.

It should be noted that the effect of flow direction of the plastic strain in forming limits prediction has been intensively investigated by many researchers (for example, Kuroda and Tvergaard, 2000a; Yoshida et al., 2007; Yoshida and Suzuki, 2008). It is not the intention of the current study to investigate the non-normality effect of plastic flow on forming limits.

2. Review of Yoshida–Uemori model

The behavior of metals under cyclic plastic deformation is quite complex. In particular, the behavior during reverse loading is usually different from the behavior in continuous loading. Yoshida and Uemori (2002) proposed a constitutive model capable of describing the deformation behavior of large-strain cyclic plasticity with its root on two-surface models. In this model, the early re-yielding phenomenon, transient Bauschinger and permanent softening effect observed from steel and aluminum material cyclic loading responses can be predicted through the Y–U model as illustrated in Fig. 2(a). It assumes a pure kinematic hardening of the yield surface within the bounding surface of mixed isotropic-kinematic hardening. Under these two-surface assumptions, a new Hardening Control Surface is constructed to control the motion and expansion of the bounding surface for the work-hardening stagnation phenomenon in reverse loading experiments as illustrated in Fig. 2(b). In Fig. 2(b), S is the deviatoric stress tensor.

Based on the assumption of a small elastic and large plastic deformation, the main frame work can be expressed as:

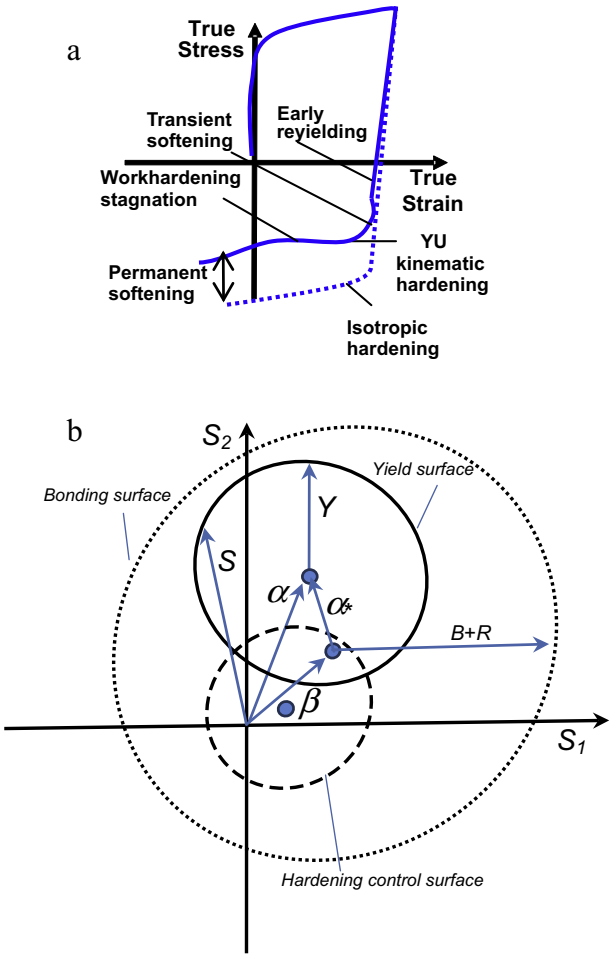

Fig. 2. Illustration of (a) the complex material response in reverse loading process and (b) the evolution of three surfaces Y–U model.

$$\mathbf{D} = \mathbf{D}^e + \mathbf{D}^p \tag{1}$$

where $\mathbf{D}$ represents the rate of deformation, $\mathbf{D}^e$ and $\mathbf{D}^p$ are the elastic and plastic parts of the rate of deformation, respectively. The constitutive law of elasticity is expressed as the equation:

$$\overset{\circ}{\boldsymbol{\sigma}} = \dot{\boldsymbol{\sigma}} - \boldsymbol{\Omega}\boldsymbol{\sigma} + \boldsymbol{\sigma}\boldsymbol{\Omega} = \mathbf{C} : \mathbf{D}^e \tag{2}$$

where $\boldsymbol{\sigma}$, $\dot{\boldsymbol{\sigma}}$ and $\boldsymbol{\sigma}\circ$ are the Cauchy stress tensor, the stress rate tensor and the objective stress rate tensor, Ω is a spin tensor, and $\mathbf{C}$ denotes the elasticity modulus tensor.

The constitutive model of plasticity is constructed within the two-surface model. Based on the Hill's48 yield criterion and associated flow rule, the flow equations are given by:

$$f(\boldsymbol{\sigma} - \boldsymbol{\alpha}) - Y = 0 \tag{3}$$

$$\mathbf{D}^p = \dot{\lambda}\frac{\partial f}{\partial(\boldsymbol{\sigma} - \boldsymbol{\alpha})} \tag{4}$$

where $\boldsymbol{\alpha}$ denotes the back stress tensor, and Y is the radius of the yield surface in the stress space. According to the Xia (2001), the Hill'48 yield criterion takes the form:

$$f(\boldsymbol{\sigma} - \boldsymbol{\alpha}) - Y = \sqrt{\frac{3}{2}(\boldsymbol{\sigma} - \boldsymbol{\alpha})^T\mathbf{P}(\boldsymbol{\sigma} - \boldsymbol{\alpha})} - Y \tag{5}$$

where $\mathbf{P}$ is defined as the plasticity matrix with anisotropic coefficients to describe different texture orientations of the material. For plane stress deformation with in-plane transverse isotropy of average r-value, $\mathbf{P}$ is

$$\mathbf{P} = \frac{2}{3}\begin{bmatrix} 1 & -\frac{r}{1+r} & 0 \\ -\frac{r}{1+r} & 1 & 0 \\ 0 & 0 & \frac{2(1+2r)}{1+r} \end{bmatrix} \tag{6}$$

The bounding surface is given by:

$$F_{bounding} = f(\boldsymbol{\sigma} - \boldsymbol{\beta}) - (B + R) = \sqrt{\frac{3}{2}(\boldsymbol{\sigma} - \boldsymbol{\beta})^T \mathbf{P} (\boldsymbol{\sigma} - \boldsymbol{\beta})} - (B + R) \tag{7}$$

where $\boldsymbol{\beta}$ denotes the center of the bounding surface, and B and R are its initial size and isotropic hardening component.

The relative kinematic motion of the yield surface with respect to the bounding surface is expressed by,

$$\boldsymbol{\alpha}_* = \boldsymbol{\alpha} - \boldsymbol{\beta} \tag{8}$$

The evolution of $\boldsymbol{\alpha}_*$ can be presented as,

$$\dot{\boldsymbol{\alpha}}_* = c\left[\frac{2}{3} a \mathbf{D}^p - \boldsymbol{\alpha}_* \dot{p}\right] \tag{9}$$

The parameters in above equation are defined as:

$$\dot{p} = \sqrt{\frac{2}{3}\mathbf{D}^p : \mathbf{D}^p}; \quad a = B + R - Y \tag{10}$$

For the center of kinematic hardening of the bounding surface, the following evolution equation is assumed:

$$\dot{\boldsymbol{\beta}} = m\left[\frac{2}{3} b \mathbf{D}^p - \boldsymbol{\beta}\dot{p}\right] \tag{11}$$

where m and b denote the material constants. The initial position of the bounding surface is located at the origin of the stress space, so $\boldsymbol{\beta}(0) = 0$.

The evolution equation of proposed isotropic hardening of the bounding surface is assumed as:

$$\dot{R} = m(R_{sat} - R)\dot{p} \tag{12}$$

where R_{sat} is the saturated value of the isotropic hardening stress R at infinitely large strain.

Due to the continuous strain hardening behavior phenomenon in material cyclic loading test, especially for advanced high-strength steels, Shi et al. (2008) proposed the use of non-saturated hardening function in Y–U model, which also gives a good agreement with experimental results of material cyclic test. Thus the evolution of R is modified as:

$$\dot{R} = nR\dot{p}/(\varepsilon_0 + p) \tag{13}$$

where n is the n-value of the material measured from uniaxial tension test, and ε_0 and p denote the initial yield strain and total equivalent plastic strain, respectively. This non-saturated hardening function will be used throughout this paper.

For describing the work hardening stagnation phenomenon, which is caused by the dissolution of dislocation cell walls during a reverse deformation, a non-isotropic hardening surface g_σ is proposed in stress space to control the global work hardening, as:

$$g_\sigma(\boldsymbol{\beta}, \mathbf{q}, r) = \frac{3}{2}(\boldsymbol{\beta} - \mathbf{q}) : (\boldsymbol{\beta} - \mathbf{q}) - r^2 = 0 \tag{14}$$

where $\mathbf{q}$ and r denote the center and the radius of the non-isotropic hardening surface, respectively. The center of g_σ is assumed to move in the direction of $(\boldsymbol{\beta} - \mathbf{q})$, following the equation:

$$\dot{\mathbf{q}} = \mu(\boldsymbol{\beta} - \mathbf{q}) \tag{15}$$

Here the parameter μ is obtained from the requirement that the center point of bounding surface should be either on or inside the surface g_σ,

$$\mu = \frac{3(\boldsymbol{\beta} - \mathbf{q}) : \dot{\boldsymbol{\beta}}}{2r^2} - \frac{\dot{r}}{r} \tag{16}$$

The evolution equation for r is given by:

$$\dot{r} = h\Gamma, \Gamma = \frac{3(\boldsymbol{\beta} - \mathbf{q}) : \dot{\boldsymbol{\beta}}}{2r} \quad \text{when } \dot{R} > 0 \tag{17}$$

$$\dot{r} = 0 \text{ when } \dot{R} = 0 \tag{18}$$

where h $(0 \leqslant h \leqslant 1)$ denotes a material parameter that determines the rate of expansion of surface g_σ. The initial value of r is assumed to be zero since the hardening stagnation will appear with reverse loading. Detailed discussion was given by Yoshida and Uemori (2002) and Yoshida et al. (2002).

3. Review of the M–K approach for forming limit prediction

The original M–K model assumes a pre-existing thickness imperfection in the form of a groove perpendicular to the principal strain direction in sheet metal. The strain localization occurs in the region of the groove. According to Hutchinson and Neale (1978), the groove should rotate during the deformation and the forming limits can be calculated based on the physical-based minimum energy principle. Kuroda and Tvergaard (2000b) imposed anisotropic coordinates of the material into the M–K model to evaluate the r-value effect in FLD. As noted earlier, this paper's focus is on the path-dependent effect. We will assume the sheet metal is transversely isotropic, and the anisotropic coordinate is the same as the loading coordinate of the sheet metal. A detailed sketch is shown in Fig. 3. The sheet metal is divided into two regions which are respectively denoted by 'a' as the normal region and 'b' as the weak region. The size of the imperfection can be defined as the initial thickness ratio $\zeta = t_0^b/t_0^a$, where 't' denotes the thickness and subscript '0' denotes the initial state. Either proportional or non-proportional loading can be imposed on the normal region to drive the deformation of the sheet.

The compatibility and equilibrium conditions connect strain and stress conditions between two regions. The compatibility equations can be expressed as:

$$\Delta\varepsilon_{tt}^a = \Delta\varepsilon_{tt}^b \tag{19}$$

where n and t denote the coordinate in the groove, $\Delta\varepsilon_{tt}^a$ and $\Delta\varepsilon_{tt}^b$ are the strain increments along the groove respectively in region 'a' and 'b'.

The force equilibrium equations across the imperfection groove are:

$$F_{nn}^a = F_{nn}^b \text{ and } F_{nt}^a = F_{nt}^b \tag{20}$$

where F is the force per unit width.

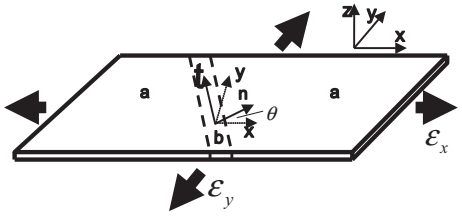

Fig. 3. A thin sheet metal with M–K analysis.

The strain increment ratio ρ is defined as an important parameter to control the strain paths, it is defined as:

$$\rho = \frac{\Delta\varepsilon_y^a}{\Delta\varepsilon_x^a} \tag{21}$$

During the deformation, the angle of the weak band should be updated as:

$$\tan(\theta + \Delta\theta) = \tan(\theta)\frac{1 + \Delta\varepsilon_x^a}{1 + \Delta\varepsilon_y^a} \tag{22}$$

In this work, the strain increment $\Delta\varepsilon_x^a$ is fixed as 0.0001 and the necking is considered to occur when the strain increment $\Delta\varepsilon_{nn}^b$ in weak band is 100 times bigger than the strain increment $\Delta\varepsilon_{nn}^a$ in normal region, i.e.

$$\frac{\Delta\varepsilon_{nn}^b}{\Delta\varepsilon_{nn}^a} > 100 \tag{23}$$

Based on the rotation angle and necking criterion established in Eqs. (22) and (23), we determine the Forming Limit as follows: first we calculate ε_x^a for given initial band angle θ, varying from 0° to 90° at intervals of 1°; then, compare all Forming Limit Values and find the minimum value of ε_x^a, and determine the corresponding components such as stresses in normal region σ_x^a, σ_y^a and effective strain in normal region ε_e^a. Smaller intervals in rotation and incremental strain step $\Delta\varepsilon_x^a$ are also examined, but no discernible difference can be observed in FLD, FLSD and epFLD.

If isotropic hardening model is adopted, the current stress state of both regions a and b can be calculated as follows:

$$\Delta\boldsymbol{\varepsilon} = \Delta\boldsymbol{\varepsilon}^{el} + \Delta\boldsymbol{\varepsilon}^{pl} \tag{24}$$

$$\boldsymbol{\sigma}^* = \mathbf{D}^{el} \cdot (\boldsymbol{\varepsilon}^{el} + \Delta\boldsymbol{\varepsilon}) \tag{25}$$

$$\Delta\boldsymbol{\varepsilon}^{pl} = \Delta\varepsilon_e \frac{\partial f}{\partial \boldsymbol{\sigma}} = \Delta\varepsilon_e \frac{3}{2\sigma_e}\mathbf{P}\boldsymbol{\sigma} \tag{26}$$

$$\boldsymbol{\sigma} = \left(\mathbf{I} + \frac{3\Delta\varepsilon_e}{2\sigma_e}\mathbf{D}^{el}\mathbf{P}\right)^{-1}\boldsymbol{\sigma}^* \tag{27}$$

where ε^{el} and $\Delta\boldsymbol{\varepsilon}$ denote the total elastic strain and strain increment vectors, respectively. The strain increment vectors are the addition of elastic strain increment vectors and plastic strain increment vectors. $\mathbf{D}^{el}$is the elastic modulus matrix, and $\mathbf{I}$ is the unit tensor. $\Delta\varepsilon_e$ is the equivalent plastic strain increment, $\mathbf{P}$ is the plasticity matrix derived from the yield surface as expressed earlier, σ_e is the effective stress and is related to the effective strain from uniaxial tensile tests. $\boldsymbol{\sigma}^*$ and $\boldsymbol{\sigma}$ are trial stress tensor and current stress state tensor, respectively. The standard radial-return mapping is used here. Initially the strain increment is assumed to be elastic to obtain the trial stress. The trial stress is used to test the yield condition with yield criterion. If the material is under plastic loading at this increment, the isotropic constitutive equations can be solved with one unknown factor, the equivalent plastic strain increment. The detailed discussion of this numerical method was given by He et al. (2013a) and He et al. (2013b).

When the Y–U kinematic hardening model is employed, the calculation process is illustrated as follows: first, with the applied tensile strain increments $\Delta\varepsilon_x^a, \Delta\varepsilon_y^a$ and initial band angle θ, the equivalent plastic strain increment in region a is calculated through Y–U model. Then, all stress states and force value in this region are obtained. Applying the force equilibrium conditions in Eq. (20) and compatibility condition in Eq. (19), only $\Delta\varepsilon_{nn}^b$, $\Delta\varepsilon_{nt}^b$ are two unknown factors for current loading step. The numerical Jacobian matrix is constructed with Y–U constitutive model, and then the Newton–Raphson method is adopted lastly to solve $\Delta\varepsilon_{nn}^b, \Delta\varepsilon_{nt}^b$ values until the force equilibrium is achieved. Details of the Y–U model was also given by He et al. (2013c).

4. Results and discussion

For the purpose of investigating the strain path effect in FLD, we consider two different scenarios of two step strain paths in which the strain increment ratio ρ is changed from (see Fig. 4):

Scenario 1: $\rho_1 = -0.5$ and ρ_2 ranges from −0.5 to 1.0;

Scenario 2: $\rho_1 = 1.0$ then ρ_2 ranges from −0.5 to 1.0.

ρ_1 and ρ_2 are defined as the first step strain increment ratio and the second step strain increment ratio, respectively.

For each of these two scenarios, we consider two different loading procedures for transitioning from the first step to the second step:

Loading condition A (“unloading” step in transition stage): first the material is loaded with the first strain increment ratio ρ_1 to a certain strain value in normal region ε_x^a; undergoes elastic unloading until the elastic strains at the normal region vanish; and then reloaded with strain increment ratio ρ_2 until the forming limit is reached;

Loading condition B (“continuous loading” in transition stage): first the material is loaded with strain increment ratio ρ_1 to a strain value in normal region ε_x^a, then the strain increment ratio is abruptly changed to ρ_2 without any unloading.

4.1. Material parameters

The same basic material properties are adopted for two different constitutive models to facilitate comparison. The uniaxial stress–strain curve is shown in Fig. 5 and material parameters for Y–U model are presented in Table 1.

Applying the volume-constancy condition and ignoring the negligible value in elastic strain of volume change in this analysis for simplicity, the other values of material constants are set as:

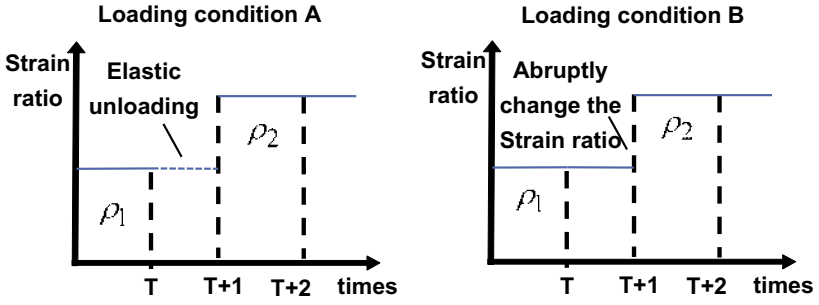

Fig. 4. The illustration of the two different loading procedures.

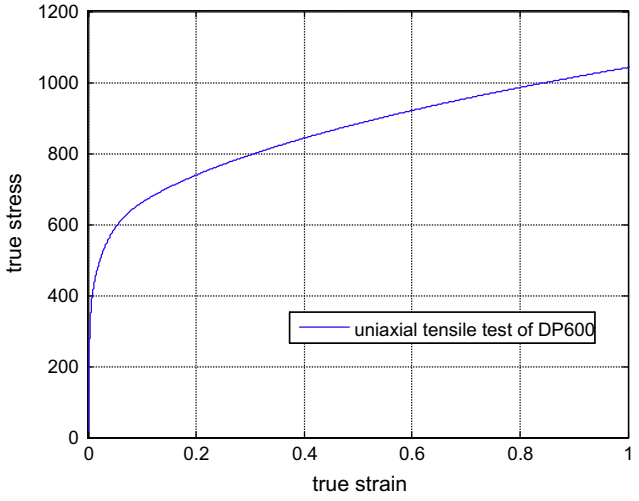

Fig. 5. The uniaxial stress–strain curve for isotropic and kinematic hardening models.

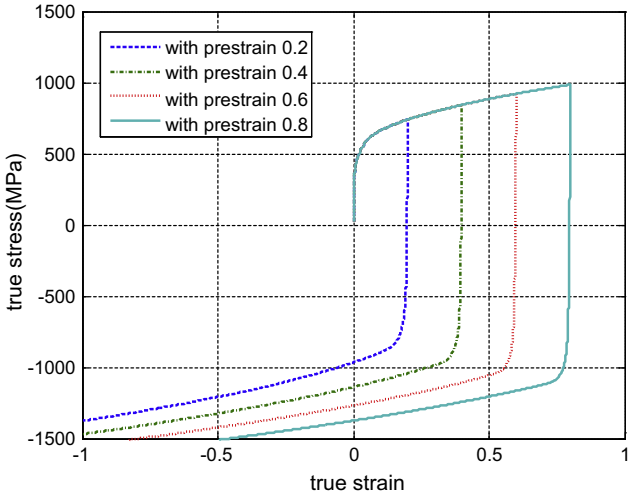

Fig. 6. The calculated uniaxial tension and compression test with different pre-strains for DP600 from kinematic hardening model.

Young's modulus E = 210 GPa, Possion's ratio $v = 0.5$. Since the r-value effect on forming limits is not included in this study, it is set to 1 for all scenarios in this paper. In the M–K analysis, the initial thickness imperfection ratio ζ is assumed to be 0.999.

Based on material parameters listed above, uniaxial tension–compression results calculated with different pre-strain levels through the modified Y–U constitutive model, the Bauschinger effect in reverse loading process such as the early re-yielding, work-hardening stagnation and permanent softening phenomenon is clearly showed in Fig. 6.

4.2. Forming limits under linear strain paths

First of all, FLD, FLSD and epFLD are studied with the same material input under both isotropic and kinematic hardening assumptions with linear strain paths. Results are shown in Figs. 7–9 with the Forming Limit Curves presented as FLD, FLSD and epFLD. Evidently no appreciable differences can be found between the forming limits with isotropic hardening assumption and those with kinematic hardening assumptions for all three criteria. This is consistent with previous reports in the literature and is consistent with our understanding.

4.3. Forming limits under nonlinear strain paths

4.3.1. Forming limits under nonlinear strain paths for scenario 1

The results for loading condition under scenario 1 are presented first. Two different loading procedures are also compared under both isotropic and kinematic hardening assumptions. In all figures, "uni" denotes the first step strain increment ratio of uniaxial loading where $\rho_1 = -0.5$ and the second step strain increment ratio ρ_2 ranges from −0.5 to 1.0. The number after the "uni" is the strain value ε_x^a right before the change of strain paths. The results from loading condition A are presented with label "unloading" in figures and the loading condition B without this label. Four pre-strain levels for the first step are studied. They are: "uni0.05", "uni0.10", "uni0.20" and "uni0.25". All FLSDs and epFLDs under

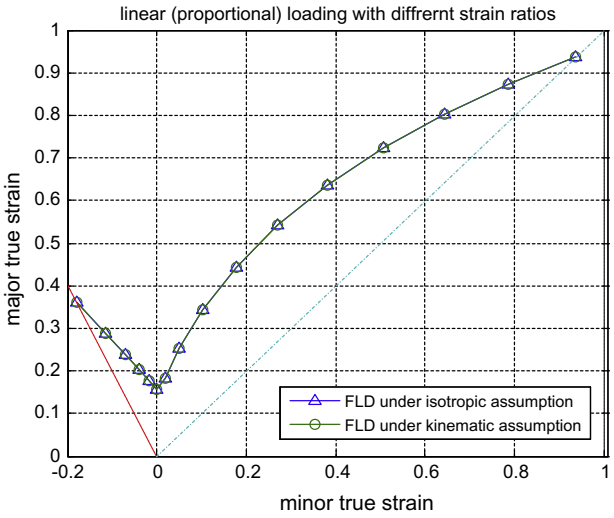

Fig. 7. The FLDs from isotropic and kinematic hardening models under proportional loading.

isotropic hardening are shown in Fig. 10 from (a) to (d); and the results from kinematic hardening are shown in Fig. 11 from (a) to (d).

It is observed from Figs. 10 and 11 that, if the amount of the pre-strain is small, the FLSD and epFLD are almost the same as the corresponding FLSD and epFLD under linear strain paths for both with-unloading and without-unloading procedures. This observation is consistent with Stoughton and Zhu (2004) and Yoshida et al. (2007).

But if the amount of the pre-strain is large enough, the nonlinear strain path effect can be found in scenarios with both isotropic and kinematic hardening assumptions. In Fig. 10(a)–(d) and 11(a)–(d), it seems the different loading procedures give larger impact on FLSD and epFLD under isotropic hardening than kinematic hardening.

It is interesting to note that, both the FLSD and epFLD results in large pre-strain scenarios under isotropic hardening (refer to

Table 1
Material parameters of DP600 for Y–U model from Shi et al. (2008).

Material	Y (MPa)	B (MPa)	C	m	b (MPa)	h	K (MPa)	N	e_0
DP600	258.8	368.8	471	45.5	163.0	0.9	605.5	0.44	0.016

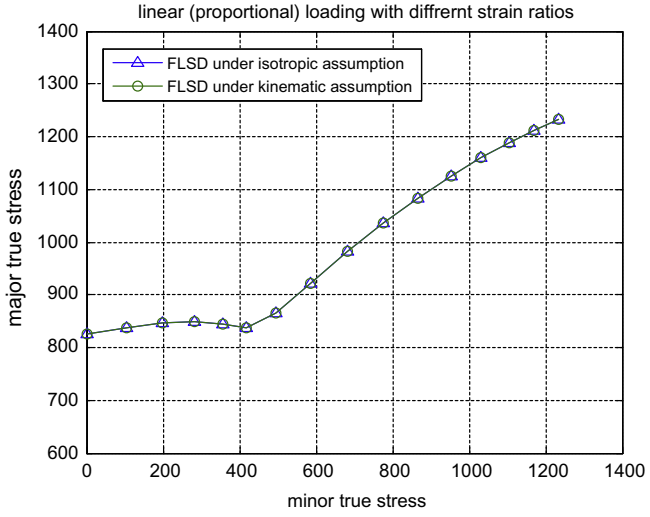

Fig. 8. The FLSDs from isotropic and kinematic hardening models under proportional loading.

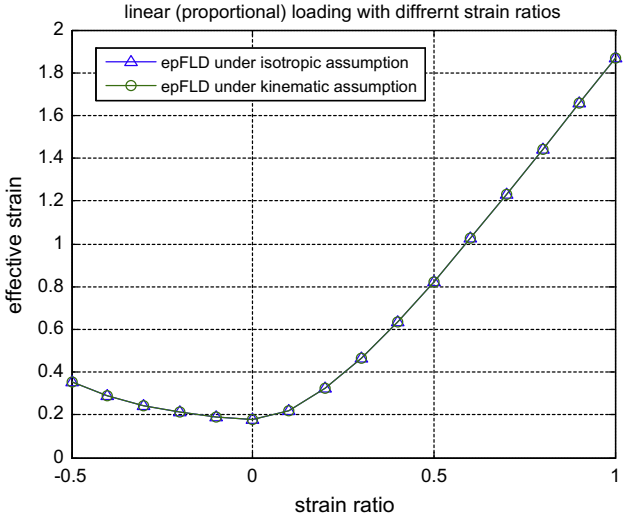

Fig. 9. The epFLDs from isotropic and kinematic hardening models under proportional loading.

results in Fig. 10a and b) show a strong path dependence, which is in contradiction to our common understanding that both the FLSD and epFLD should be path-independent. Yoshida et al. (2007) offered a plausible explanation. They found that if the unloading process is not considered after the first step loading, the transition stage (abruptly change the strain increment ratio after the first step) that we imposed in the M–K analysis causes a big impact on the defect, and therefore on the final necking state. Since the

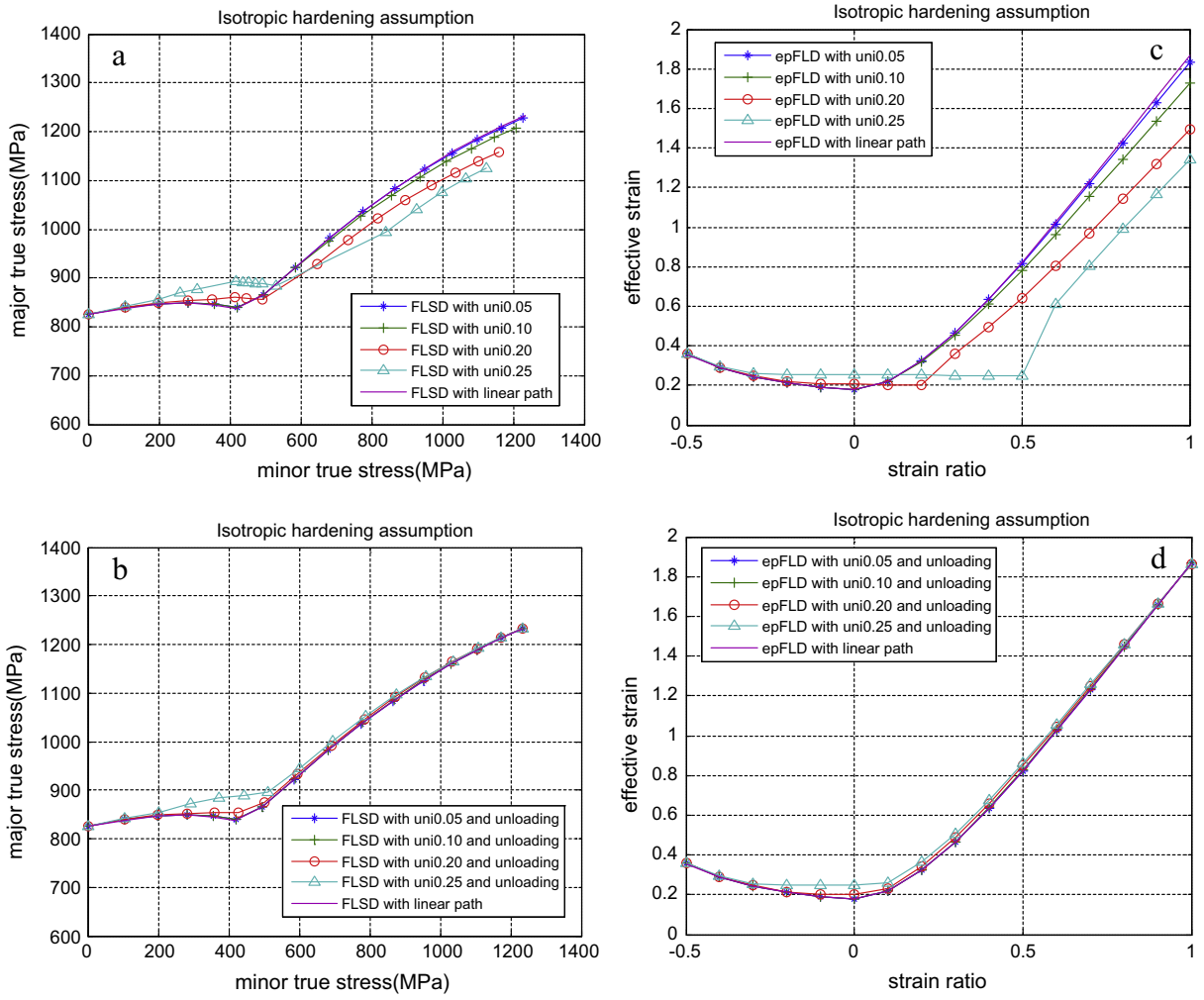

Fig. 10. The results from isotropic hardening model under non-proportional loading with $\rho_1 = -0.5$.

M–K analysis is based on the damage (or defect) accumulation methodology, the necking occurs when the final damage reaches a critical state. Anything affecting the defect evolution will be reflected in the Forming Limit at the end in M–K analysis. Consequently the path-independent understanding of FLSD and epFLD under isotropic hardening cannot be interpreted the same way when the M–K analysis is employed. The detailed information of the effect from transition stage on damage accumulation and stress evolution is discussed in scenario study of Section 4.3.3.

4.3.2. Forming limits under nonlinear strain paths for scenario 2

The results of the scenario 2 are presented in Figs. 12 and 13. Following notations we used earlier, "bia" denotes first step biaxial loading where the strain increment ratio ρ_1 equals to 1.0, and then the second step strain increment ratio ρ_2 ranges from −0.5 to 1.0 for a full FLD curve. The numbers after the "bia" is again the strain value ε_x^a right before the change of strain paths. Four strain levels for the first step are calculated as: "bia0.10", "bia0.30", "bia0.50" and "bia0.70". All FLDs, FLSDs and epFLDs under isotropic hardening assumption are shown in Fig. 12 from a to d. The results from kinematic hardening assumption are shown in Fig. 13 from a to d.

With small amount of pre-straining, similar results can be observed for both FLSD and epFLD as shown in Fig. 12(a)–(d) and Fig. 13(a)–(d). In Fig. 12(b) and (d), data points denoted with "necking occurs at the start of second loading" means that the necking occurs just upon re-yielding of the second loading process. It seems that the different loading procedures are more important for FLSD in scenario 2. Path-dependence is evident in Figs. 12(a) and (b) and 13(a) and (b) for FLSD in large pre-strain scenarios due to the unloading process. The epFLDs in Figs. 12(c) and (d) and 13(c) and (d) show that if the first step loading gives higher effective strain than that under the linear strain path, then the necking occurs right at the start of the second step loading. If we consider strain history effect in forming limits in this manner, both the FLSD and epFLD are path-dependent under isotropic and kinematic hardening assumptions with the different loading procedures, especially the first step loading is biaxial stretch.

The results on Figs. 12(c) and (d) and 13(c) and (d) indicate that the epFLD is more insensitive to the loading conditions than the FLSD. In the metal forming operation, the complex loading processes are imposed into sheet metals with the different strain paths. So epFLD may provide more "path-independent" properties for assessing the necking failure.

In Sections 4.3.1 and 4.3.2, the two-step strain path deformation mode is adopted with both isotropic and Y–U kinematic hardening models for the detailed investigation of path dependence phenomenon in forming limits. The goal here is to compare two general path-independent forming limits FLSD and epFLD for industrial applications. If M–K analysis is employed to study this problem, then the damage (or defect) accumulation assumption inevitably exists in localized necking evolution, which seems to be the important reason for the path dependence phenomenon in M–K analysis.

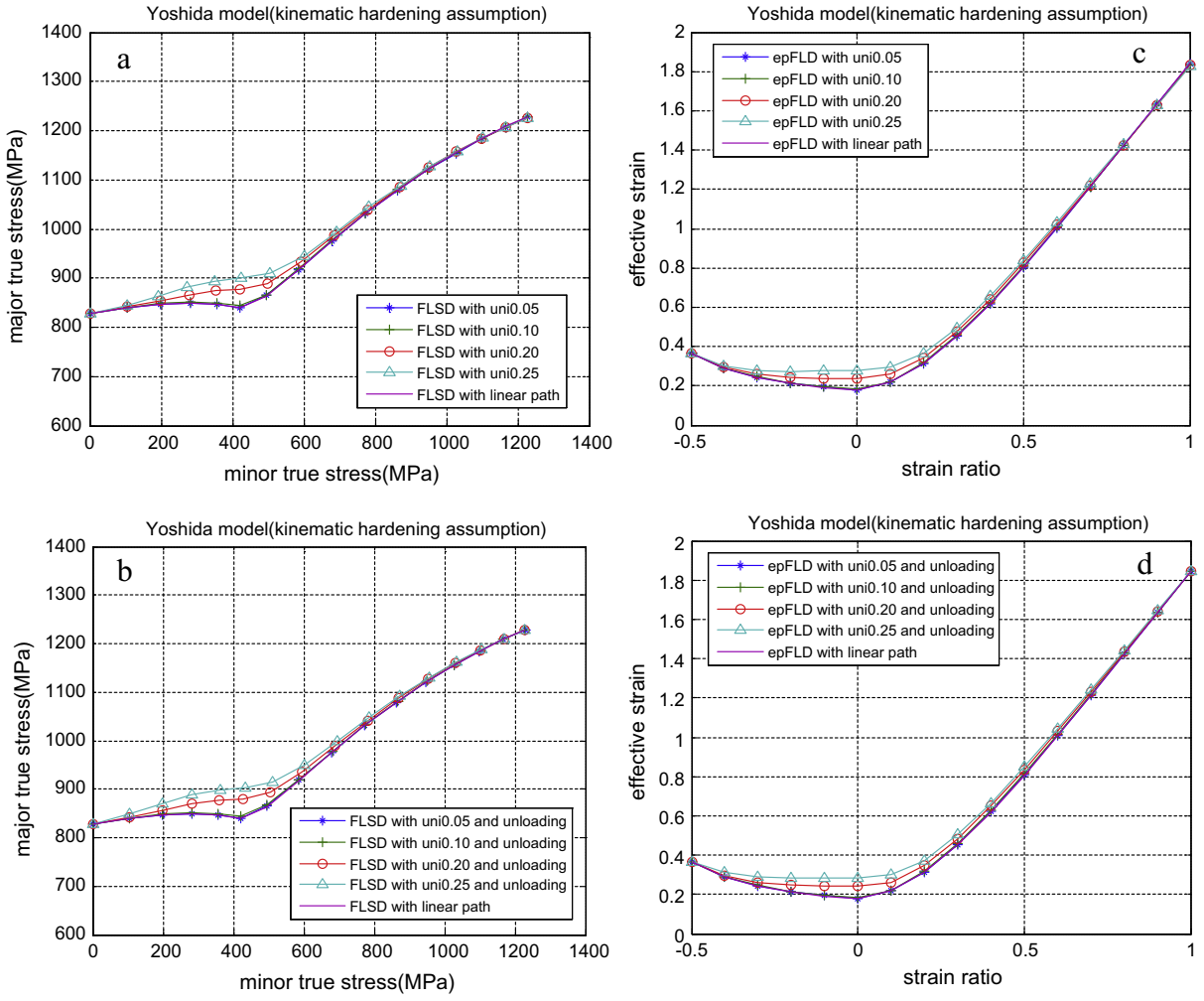

Fig. 11. The results from kinematic hardening model under non-proportional loading with $\rho_1 = -0.5$.

If this damage accumulated assumption is physically true for sheet metal instability, then the pre-imposed damage in first loading process decide the final result of forming limits for both FLSD and epFLD.

4.3.3. The influence of the loading history and Bauschinger effects on forming limits as predicted by the M–K analysis

To understand the nonlinear strain path effect on forming limits predicted above, we set to investigate in greater details the influence of loading histories and kinematic hardening effects as predicted by M–K analysis. Without the loss of generality, we select two loading scenarios and examine their stress evolutions. The first one is the scenario presented in Fig. 14(a) and (b) with label "bia", where the material is loaded with the strain increment ratio $\rho_1 = 1.0$ to a certain value ε_x^a, then reloaded with the strain increment ratio $\rho_2 = -0.5$ until the localized necking occurs. The unloading process after the first loading step is also considered as shown in Fig. 14(c) and (d). The scenarios studied with or without unloading step under isotropic and kinematic hardening can be listed as below:

(1) $\rho_1 = 1.0$, then $\rho_2 = -0.5$,
(2) $\rho_1 = 1.0$, then apply unloading step (unload all elastic strain), after that $\rho_2 = -0.5$,

The Fig. 14 shows the stress trajectories of the scenarios "bia0.10", "bia0.30" and "bia0.70" under continuous loading or with unloading step in transition stage between two different strain paths. Label "continuous loading" will be used to denote the loading condition B and "with unloading" will be denoted the loading condition A. Black points are the necking points under these conditions.

As can be observed in Fig. 14(a), stress evolutions under the continuous loading condition are similar after the strain increment ratio is abruptly changed. All stress paths under this loading condition move on the current yield surface, which is considered as the most unstable deformation mode. The material undergoes the "plastic" plane strain stretching mode as presented in Yoshida et al. (2007). The similar phenomenon is observed by Kuroda and Tvergaard (1999) under isotropic hardening assumption for the yield surface measurement, and the detailed experimental results of the yield surface measured through this loading condition (abruptly change the strain increment ratio at second step loading without unloading step) are published by Kuwabara et al. (2000).

Results obtained here indicate that this unstable deformation mode also exists under two-surface kinematic hardening assumption as presented in Fig. 14(b). The deformation becomes stable again after the stress passes the unstable mode on yield

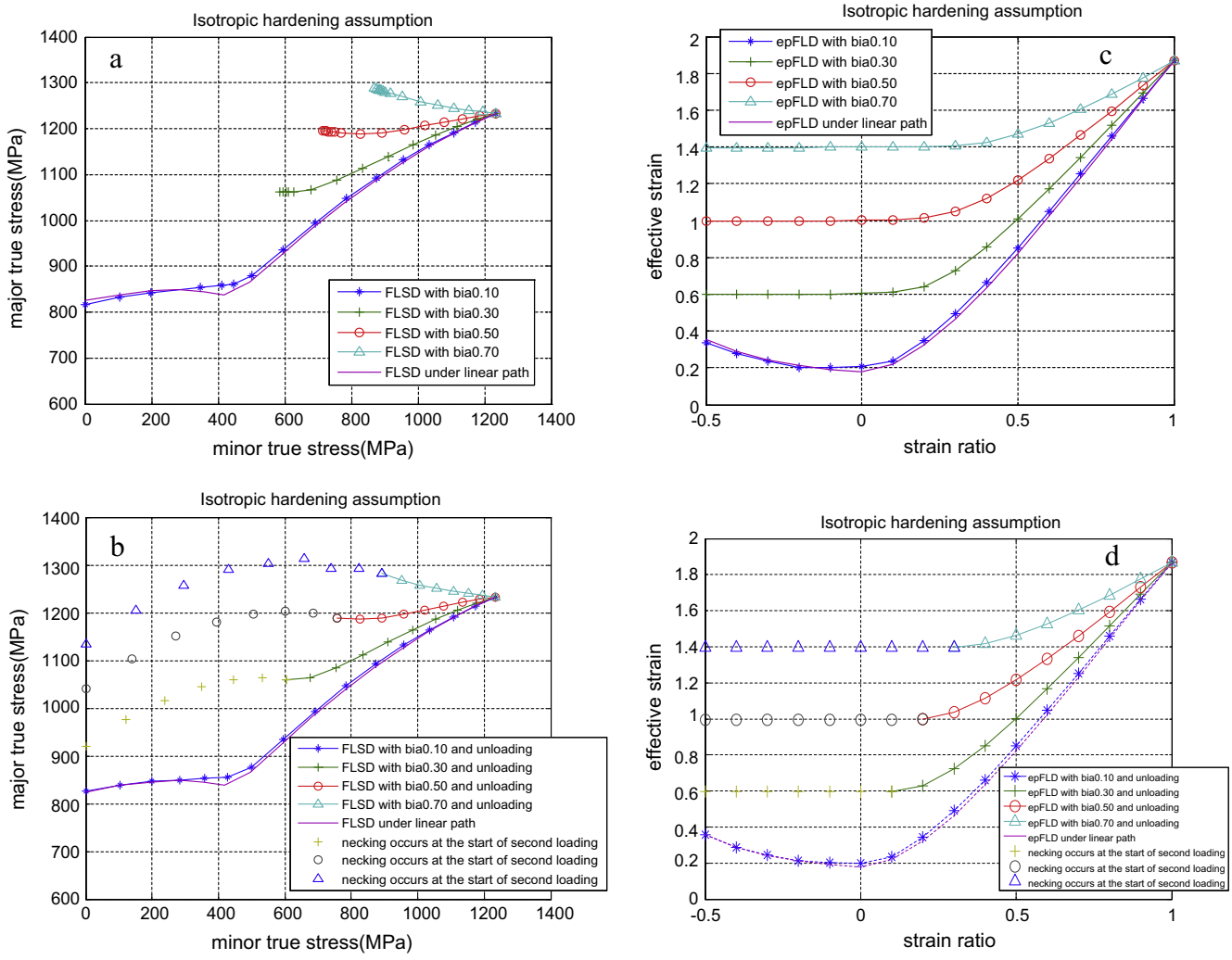

Fig. 12. The results from isotropic hardening model under non-proportional loading with $\rho_1 = 1.0$.

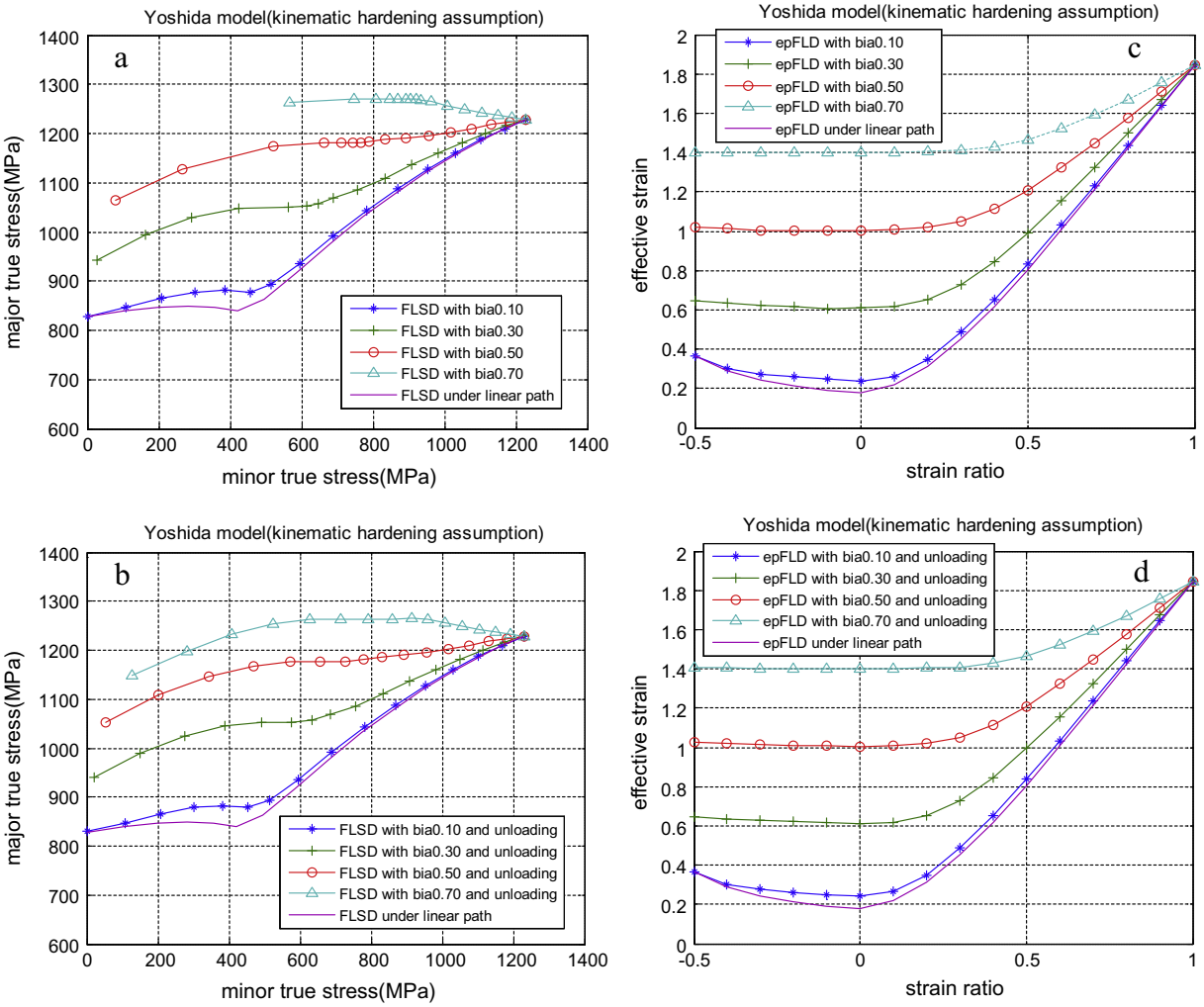

Fig. 13. The results from kinematic hardening model under non-proportional loading with $\rho_1 = 1.0$.

surface. It seems that the stress path changes nonlinearly until it reaches the assigned strain increment ratio as if it were moving on the yield surface. Based on the Fig. 14(a) and (b), more sharp change in transitioning stress trajectory when it leaves the yield surface can be observed in continuous loading scenarios under isotropic than kinematic. This difference comes from the material's Bauschinger effect in stress–strain response as illustrated in the Fig. 15. The circle, rectangle and triangle in the Fig. 15(b) and (c) correspond to those in the Fig. 14(a) and (b). Continuous hardening can be observed in isotropic hardening scenario in Fig. 15(a), but sudden softening appears in kinematic hardening scenario in same figure due to the strain path change in second step loading. Since the stress level of material predicted in kinematic hardening is smaller than that with isotropic hardening after the abrupt change of strain path, the sheet can achieve larger deformation before necking. Consequently the limit strain in the scenario of kinematic hardening is higher than that with isotropic hardening as presented in Fig. 15(a). It is evident that the constitutive law is one of the key factors in influencing forming limits under nonlinear strain path loading.

If unloading occurs following the first step loading, there is no "plastic" plane strain stretching mode in isotropic scenarios. Due to the change of the size of the yield surface, the position of the necking stress is higher than the FLSD in scenario "bia0.30" and "bia0.70" in Fig. 14(c). The relevant yield stress passes the position of FLSD in the direction of $\rho_2 = -0.5$ in stress space after the first step loading, so the localized necking occurs as soon as the material starts plastic deformation in large pre-strain scenarios after the unloading step in transition stage as illustrated in Fig. 16. As illustrated in Fig. 16, the black dots are necking points and correspond to those in the Fig. 14(c).

Under the kinematic hardening assumption, the nonlinear stress paths in Fig. 14(d) suggest that the unstable mode still affects the scenarios we investigated. The Bauschinger effect described in the constitutive law is the real reason for this phenomenon as showed in Fig. 17. In Fig. 14(d), the curves show that the material is re-yield after the unloading process, then the direction of the stress in stress space shifts step by step until the corresponding stress ratio is achieved (or the localized necking occurs in this process in Fig. 14(d)). The circle and triangle in Fig. 17(b) correspond to those in the Fig. 14(d).

If the amount of pre-strain is small, the kinematic hardening effects on later deformation will also be small, and the M–K analysis with different constitutive laws yields FLSD results more or less convergent to those under linear strain path condition. However as the pre-strain amount increases, the influences from kinematic hardening on later deformation will become more significant, resulting in more pronounced path-dependence of forming limits.

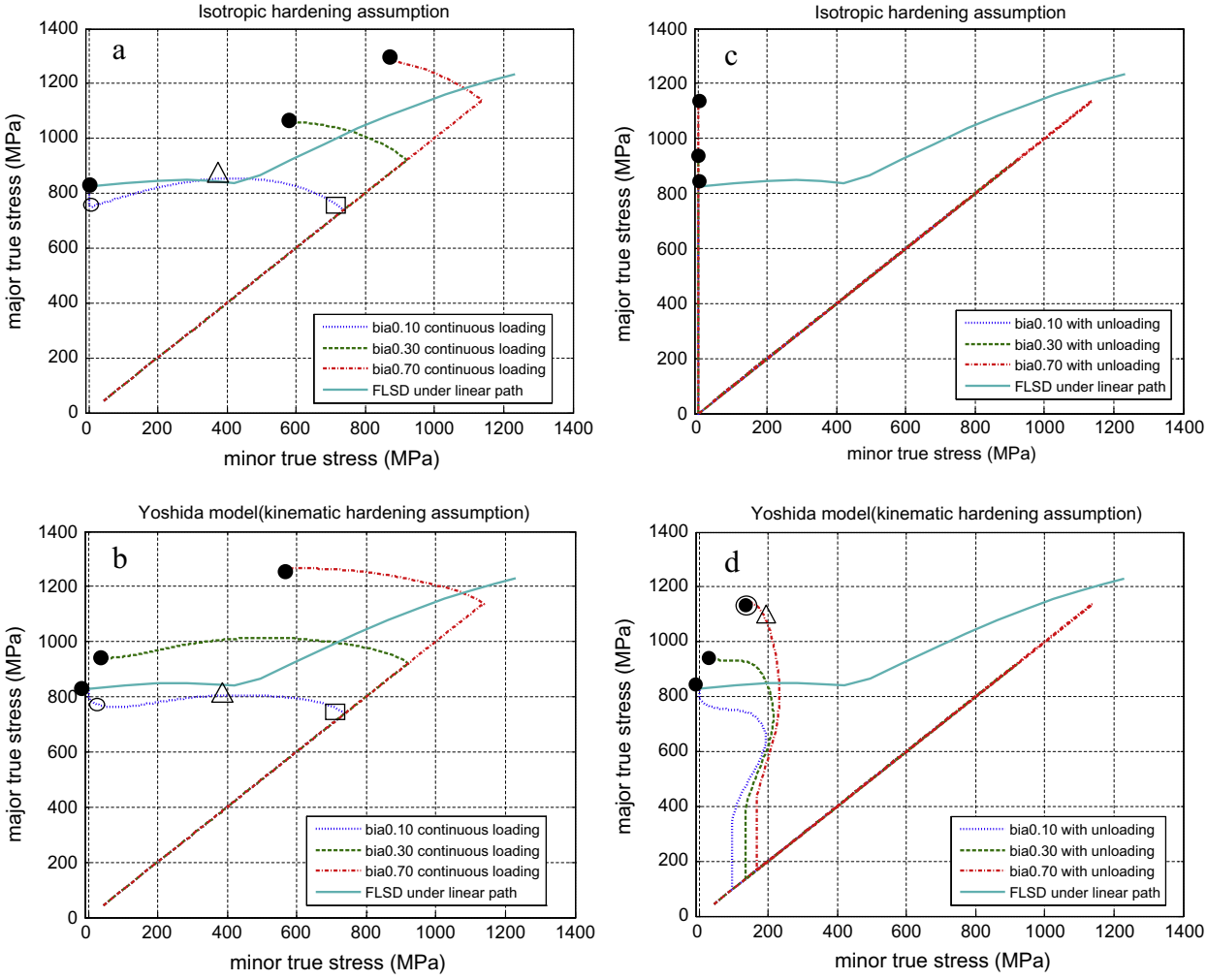

Fig. 14. The evolution of the stress under isotropic and kinematic assumptions with different loading procedures.

To further understand the influence of large pre-straining on the forming limits, the evolution of defect development in the imperfection zone is examined in great details. The development of a defect is represented by the ratio of the effective strain inside to that outside of the band as $\varepsilon_e^b/\varepsilon_e^a$ in Fig. 18. As stated earlier, "uni" and "bia" denote the scenarios with different strain path at the first step, the "with unloading" and "continuous loading" labels represent the different loading procedures as loading condition A and loading condition B in analysis.

In Fig. 18(a), under the isotropic hardening assumption, the effective strain ratio between inside and outside the band "jumps" suddenly in development of the defect. It means the weak band rapidly develops right after the strain path change, and then the defect returns to the stable evolution until the localized necking occurs. This phenomenon was also observed by Kuroda and Tvergaard (2000a) and Yoshida et al. (2007) as "pseudo-localization". Based on Fig. 18, it suggests that this strong "pseudo-localization" phenomenon only exists under the isotropic hardening condition without unloading process as presented in Fig. 18(a), no significant "pseudo-localization" phenomenon can be observed under kinematic hardening assumption in both with or without unloading process in Fig. 18(b) and (c). The results in Fig. 18 seems to show that the effective strain ratio between region a and b is more strongly influenced under the isotropic hardening than kinematic hardening if the unloading process is not considered in the loading procedure.

In Fig. 18(b) and (c), the curves for the development of a defect are so steep in large pre-strain scenarios, it seems the neck occurs right after the material is hardened enough by the first step loading. If the first loading step is biaxial stretch, the similar forming limits can be achieved in small pre-strain scenarios in both isotropic and kinematic assumptions, the development of a defect is a little different when it compares with the defect evolution under linear strain path as shown in Fig. 18(b) and (c).

For summarizing the results and discussion above, one important observation should be noted. The path-independent forming limits under isotropic assumption such as FLSD and epFLD show path-dependent phenomenon under kinematic hardening, and it can be understood as following: the softening phenomenon after the prior loading step in Bauschinger effect as well as the loading procedure in transition stage gives a big impact on the final forming limits, which means the strain path history is involved to describe the current deformation state of the material under kinematic assumption.

It seems that the path-dependent phenomenon observed from M–K analysis largely depends on the damage accumulation assumption in this defect imposed model. The constitutive law adopted in this analysis is one sensitive factor for the pre-strain inputted damage under nonlinear strain path loading conditions as illustrated by Yoshida et al. (2007). According to this point, the constitutive law is a sensitive factor for the path-dependent phenomenon under the M–K analysis, but not the major reason.

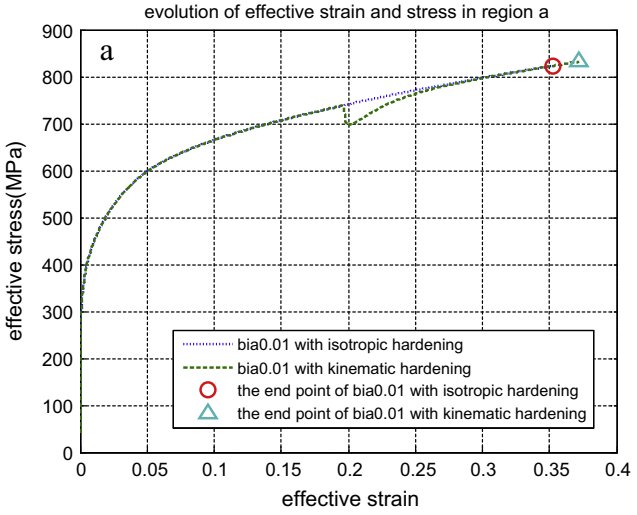

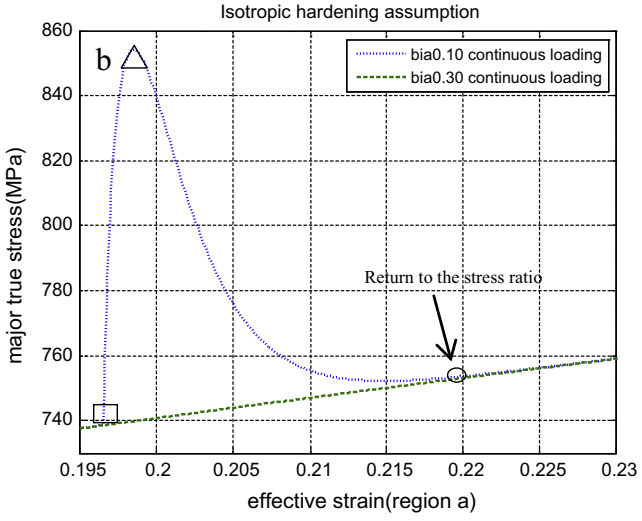

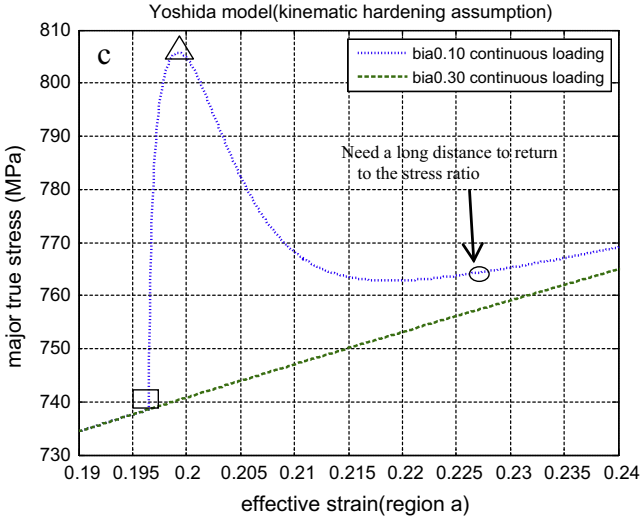

Fig. 15. The relationship between the major true stress and effective strain.

The more damage (or pre-strain) imposed into the M–K model, the stronger path-dependent phenomenon can be expected. As stated earlier, if this damage accumulated assumption is physically true for the understanding of sheet metal instability, then the quantity of pre-imposed damage as well as the damage mode in previous

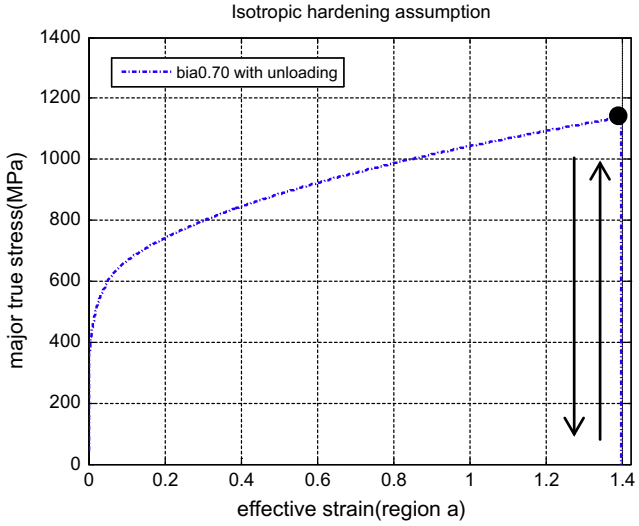

Fig. 16. The relationship between the major true stress and effective strain.

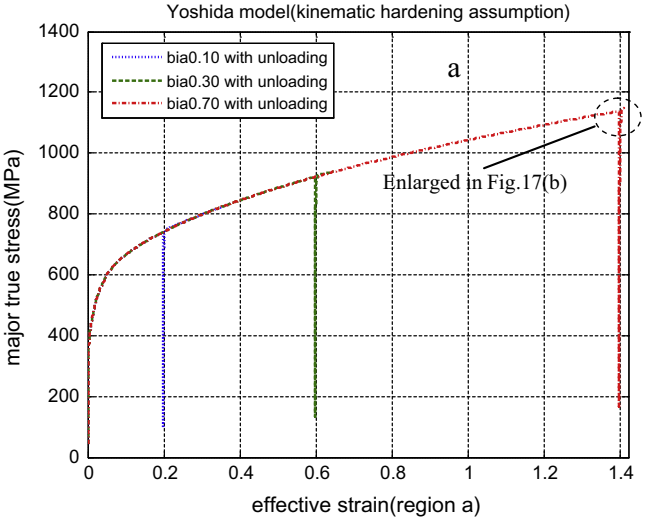

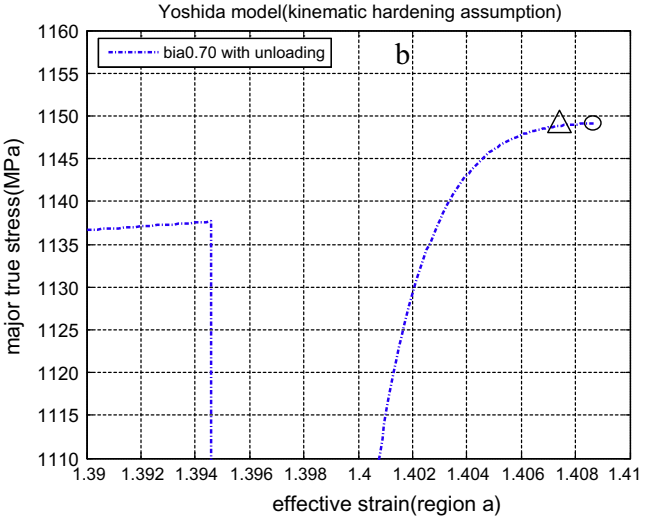

Fig. 17. The relationship between the major true stress and effective strain.

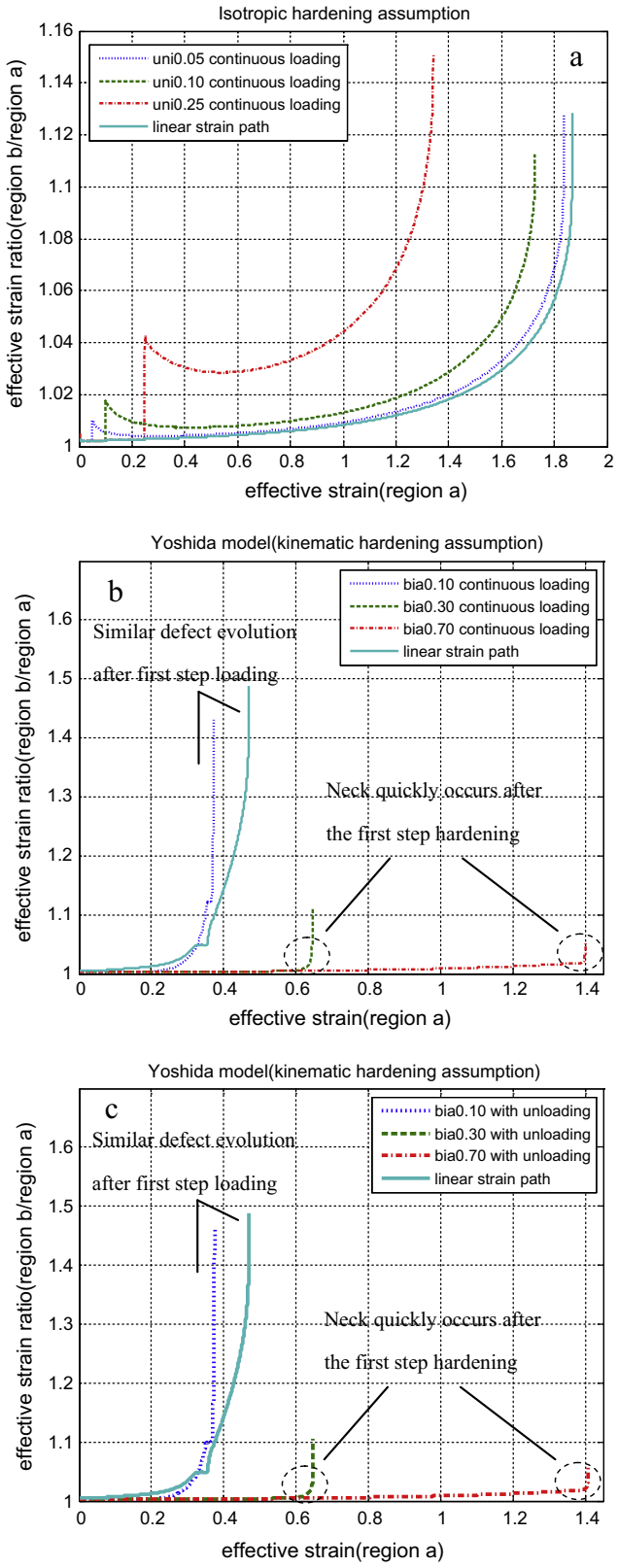

Fig. 18. The evolution of the effective strain ratio under isotropic and kinematic assumptions with different loading procedures.

loading processes decides the final state of forming limits. The tendency observed in this paper is also valid under damage accumulated assumption for necking instability.

5. Conclusions

In this study, the FLD, FLSD and epFLD with different loading procedures in transition stage are analyzed using the M–K analysis, and the nonlinear strain path effect in forming limits is discussed in detail. Both the isotropic and Yoshida's two-surface kinematic hardening model with the same Hill'48 yield surface are considered and compared against each other. The stress evolution and effective strain ratio evolution are presented to improve our understanding for this issue. The conclusions of this study can be summarized as follows:

1 Under linear strain path conditions, there are no appreciable differences in predicted Forming Limit Curves under either isotropic or kinematic hardening constitutive models, whether it is in the form of FLD, FLSD or epFLD.
2 The loading condition during the transitional stage of strain path changes plays a key role in the nonlinear strain path effect in forming limits. If the unloading step is considered, it changes stress states under both isotropic and kinematic hardening assumptions. If the continuous loading is assumed, unstable deformation mode can be observed in M–K analysis.
3 The Bauschinger effect of material's stress–strain response in the subsequent work-hardening behavior after the first step loading is important for forming limits prediction under nonlinear strain path condition due to the loading, unloading and reverse loading processes.
4 The dependence of the FLD is determined by the pre-strain level. When the effective pre-strain level is less than the effective strain at plane strain condition, the FLSD and epFLD are path independent. When the effective pre-strain is higher than the effective strain at plane strain condition, the FLSD and epFLD obtained from M–K analysis show path dependent. This path dependent phenomenon may contribute from the damage accumulation in M–K analysis, but not the constitutive law.

The current study provides a better understanding of path-dependent phenomenon on forming limits such as FLSD and epFLD under kinematic hardening assumption. Since available experimental studies in the literature have not been able to provide enough clarity on forming limits (FLSD and epFLD) under nonlinear strain path conditions, nor used to validate the path-independent forming limits of theoretical work, the insight obtained in this paper will help to further understand the influence of strain history as well as loading conditions on forming limits under both isotropic and kinematic hardening assumptions.

Acknowledgments

This study is conducted while one of the authors (Ji He) is a visiting academic at the Research & Innovation Center of Ford Motor Company in Dearborn, Michigan. Financial support from National Natural Science Foundation of China (51222505), National Natural Science Foundation of China (51075267) and Ford Motor Company through its University Research Program (URP) is gratefully acknowledged.

References

Cao, J., Yao, H., Karafillis, A., Boyce, M.C., 2000. Prediction of localized thinning in sheet metal using a general anisotropic yield criterion. Int. J. Plast. 16, 1105–1129.
Friedman, P., Houston, D., 1999. Effects of prestraining on the formability of Al–Mg sheet alloys. Ford internal technical report.
Graf, A., Hosford, W., 1993. Effect of changing strain paths on FLD. Metall. Mater. Trans. A 24, 2503–2512.
Graf, A., Hosford, W., 1994. The influence of strain-path changes on forming limit diagrams of A1 6111 T4. Int. J. Mech. Sci. 36, 897–910.

He, J., Xia, Z.C., Li, S.H., Zeng, D., 2013a. M–K analysis of forming limit diagram under stretch-bending. ASME J. Manuf. Sci. Eng. 135 (4), 0410191–04101910.
He, J., Xia, Z.C., Zeng, D., Li, S.H., 2013b. Forming limits of a sheet metal after continuous-bending-under-tension loading. ASME J. Eng. Mater. Technol. 135 (3), 0310091–0310098.
He, J., Xia, Z.C., Zhu, X.H., Zeng, D., Li, S.H., 2013c. Sheet metal forming limits under stretch-bending with anisotropic hardening. Int. J. Mech. Sci. 75, 244–256.
Hutchinson, J., Neale, K., 1978. Sheet necking-II: time-independent behavior. In: Koistinen, D.P., Wang, N.M. (Eds.), Proceedings of a Symposium of Mechanics of Sheet Metal Forming, pp. 127–150.
Keeler, S.P., 1965. Determination of forming limits in automotive stampings. SAE Paper 650535.
Keeler, S.P., Backhofen, W.A., 1964. Plastic instability and fracture in sheet stretched over rigid punches. Trans. Am. Soc. Metals 56, 25–48.
Kuroda, M., Tvergaard, V., 1999. Use of abrupt strain path change for determining subsequent yield surface: illustrations of basic idea. Acta Mater. 47, 3879–3890.
Kuroda, M., Tvergaard, V., 2000a. Effect of strain path change on limits to ductility of anisotropic metal sheets. Int. J. Mech. Sci. 42, 867–887.
Kuroda, M., Tvergaard, V., 2000b. Forming limit diagrams for anisotropic metal sheets with different yield criteria. Int. J. Solids Struct. 37, 5037–5059.
Kuwabara, T., Kuroda, M., Tvergaard, V., Nomura, K., 2000. Use of abrupt strain path change for determining subsequent yield surface: experimental study with metal sheets. Acta Mater. 48, 2071–2079.
Kuwabara, T., Yoshida, K., Narihara, K., Takahashi, S., 2005. Anisotropic plastic deformation of extruded aluminum alloy tube under axial forces and internal pressure. Int. J. Plast. 21, 101–117.
Laukonis, J.V., Ghosh, A.K., 1978. Effects of strain path changes on the formability of sheet metals. Metall. Trans. 9A, 1849–1856.
Lloyd, D.J., Sang, H., 1979. The influence of strain path on subsequent mechanical properties-orthogonal tensile paths. Metall. Trans. 10A, 1767–1772.
Shi, M.F., Zhu, X., Xia, C., Stoughton, T.B., 2008. Determination of nonlinear isotropic/kinematic hardening constitutive paramaters for AHSS using tension and compression tests. NUMISHEET 2008, 137–142.
Stoughton, T.B., 2000. A general forming limit criterion for sheet metal forming. Int. J. Mech. Sci. 42, 1–27.
Stoughton, T.B., 2001. Stress-based forming limits in sheet-metal forming. ASME J. Eng. Mater. Technol. 123, 417–422.
Stoughton, T.B., Zhu, X., 2004. Review of theoretical models of the strain-based FLD and their relevance to the stress-based FLD. Int. J. Plast. 20, 1463–1486.
Xia, Z.C., 2001. Failure analysis of tubular hydroforming. ASME J. Eng. Mater. Technol. 123 (4), 423–429.
Yao, H., Cao, J., 2002. Prediction of forming limit curves using an anisotropic yield function with prestrain induced backstress. Int. J. Plast. 18, 1013–1038.
Yoshida, K., Kuwabara, T., 2007. Effect of strain hardening behavior on forming limit stresses of steel tube subjected to nonproportional loading paths. Int. J. Plast. 23, 1260–1284.
Yoshida, K., Suzuki, N., 2008. Forming limit stresses predicted by phenomenological plasticity theories with anisotropic work-hardening behavior. Int. J. Plast. 24, 118–139.
Yoshida, F., Uemori, T., 2002. A model of large-strain cyclic plasticity describing the Bauschinger effect and workhardening stagnation. Int. J. Plast. 18, 661–686.
Yoshida, F., Uemori, T., Fujiwara, K., 2002. Elastic–plastic behavior of steel sheets under in-plane cyclic tension–compression at large strain. Int. J. Plast. 18, 633–659.
Yoshida, K., Kuwabara, T., Narihara, K., Takahashi, S., 2005. Experimental verification of the path-independence of forming limit stresses. Int. J. Form. Processes 8, 283–298.
Yoshida, K., Kuwabara, T., Kuroda, M., 2007. Path-dependence of the forming limit stresses in a sheet metal. Int. J. Plast. 23, 361–384.
Zeng, D., Chappuis, L., Xia, Z.C., Zhu, X., 2009. A path independent forming limit criterion for sheet metal forming simulations. SAE Int. J. Mater. Manuf. 1, 809.